In-situ AFM and EIS Study of a Solventborne Alkyd Coating with Nanoclay for Corrosion Protection of Carbon Steel

Jing Li[1], Luiz Ecco[2], Michele Fedel[2], Valentina Ermini[3], Gregory Delmas[4], Jinshan Pan[1]

[1]*KTH Royal Institute of Technology, School of Chemical Science and Engineering, Division of Surface and Corrosion Science, SE-100 44 Stockholm, Sweden*

[2]*Department of Industrial Engineering, University of Trento, Trento, Italy*

[3]*Laviosa Chimica Mineraria SpA, Via L. Da Vinci 21, Livorno 57123, Italy*

[4]*Arkema Coating Resins, Parc Technologique ALATA, Verneuil en Halatte, France*

*Corresponding author**.** Tel: +46-8790-9919. Fax: +46-820-8284. E-mail: jing5@kth.se

Abstract

A solventborne alkyd composite coating containing montmorillonite (MMT) nanoclay was made on carbon steel, and its corrosion protection was investigated by *in-situ* atomic force microscopy (AFM) and electrochemical impendence spectroscopy (EIS) measurements in 3 wt.% NaCl solution. X-ray diffraction (XRD) analysis indicated intercalation of MMT sheets in the composite coating. Thermo-gravimetric analysis (TGA) demonstrated improved thermal stability of the composite coating due to the nanoclay. Scanning electron microscopy (SEM) and AFM examination revealed dispersion and also some aggregation of the nanoclay particles in the coating. *In-situ* AFM images show a stable coating surface at nano-scale during relative long time exposure in the NaCl solution, indicating an excellent stability of the composite coating. The EIS results confirmed that the composite coating can provide a long term barrier-type corrosion protection for carbon steel in the corrosive solution. The good barrier type corrosion protection could be attributed to the lamellar MMT sheets in the coating that block the defects and decrease the transport of water and corrosive species.

Keywords: alkyd coating; nanoclay; corrosion protection; in-situ AFM; EIS.

1. Introduction

Polymeric coatings have been widely used for corrosion protection of metallic substrates because they are easy to apply with a reasonable cost. Among possible choices of polymeric coatings, solventborne alkyd coatings have been extensively used due to its excellent gloss, good durability as well as relatively low cost. Alkyd resins are important ingredients in the synthetic paint industry since they are useful as film forming agents in paint, varnishes and enamel plastics [1]. However, the corrosion protection of such polymeric coatings usually will fail once the coating is damaged by the formation of defects on the surface, in spite of good barrier properties and strong adhesion performance given by the alkyd matrix [2].

One of new developments in corrosion protection is to produce composite polymer coatings with enhanced barrier property, e.g., through adding nanoclay into the coatings. Recently, layered silicate materials such as montmorillonite (MMT, general formula $M_x(Al_{4-x}Mg_xSi_8O_{20}(OH)_4$) has been used for preparation of polymer-clay nanocomposite because its lamellar sheets, displaying high in-plane strength, stiffness and high aspect ratio [3][4]. Typically, the chemical structures of MMT consist of two fused silica tetrahedral sheets sandwiching an edge-shared octahedral sheet of either magnesium or aluminum hydroxide. In general, there are three different types of composite arising from the interaction of layered silicates and polymers: phase-separated microcomposite; intercalated nanocomposite and exfoliated nanocomposite. An exfoliated structure is obtained when the silicate layers are completely and uniformly dispersed in a continuous polymer matrix; an intercalated nanocomposite is built up when the polymer chains is intercalated into the silicate layers, usually along with the increase of the interlayer spacing [5][6].

It has been reported that the incorporation of lamellar pigments into polymer coatings such as polyaniline, epoxy or silane significantly improves the mechanical and barrier properties, thermal stability, wear resistance, etc. of the coating at a relative low loading of nanoclay

[7][8][9][10][11][12][13][14][15][16][17]. The improvement is essentially related to the morphology of the clay layers and the integration of the nanoparticles in the polymeric matrix [18]. Considerable efforts have been made on the preparation and investigation of corrosion protection performance of organic-nanoclay composite coatings for pure aluminum [19], cold rolled steel [15][16][17] and galvanized steel [20], however, there are limited reports about the study of corrosion protection of solventborne alkyd coatings with MMT additive.

Electrochemical techniques have been widely applied to evaluate the corrosion protection performance of polymer-clay composite coatings, mostly using open-circuit potential (OCP) and electrochemical impedance spectroscopy (EIS) measurements, while few study utilized AFM technique [21]. In recent years, AFM becomes easily available in many research laboratories. In addition to the advantage of high spatial resolution, AFM measurement can be made under liquid conditions, which can unveil detailed information of composite polymer coatings, such as processing, reaction and deformation. In the study of corrosion protection of polymer coatings, *in-situ* AFM measurement enables direct and real time monitoring of the change of surface layer taking place in corrosive solutions [22].

In this work, a solventborne alkyd composite coating (alkyd-MMT) with 3 wt.% MMT was prepared and coated on carbon steel. The alkyd clear coating samples without MMT additive were also prepared for comparison. In addition to characterization of the micro- and nano-structure and thermal stability of the composite coating, *in-situ* AFM measurements in 3 wt.% NaCl solution were performed to investigate the effect of MMT nanoclay particles in the coating on the corrosion protection performance. And, the barrier property of the composite coating was evaluated by means of EIS measurements during a long exposure period. The role of the MMT additive is discussed based on the *in-situ* AFM observations and the EIS results, as well as the micro- and nano-structure of the composite coating.

2. Experimental

2.1. XRD and TGA analyses of the coatings

The nanoclay composed of sodium MMT platelets was provided by the Laviosa Chimica Mineraria SpA, Italy. Typical particle size is 7-9 μm and the particles consist of the platelets of ca. 1 nm in thickness and a few microns in length. For preparation of the composite coating, the nanoclay was modified by an organic modifier (industrial confidential information) following the procedures: 1000 ml of concentrated nanoclay suspension was heated up to 70 °C in a beaker equipped with a mechanical stirring, and then the organic modifier was added. The reaction was stopped after 45 minutes, and the resulting product was filtered under vacuum through a synthetic tissue and then washed with fresh hot water, and finally dried and milled, yielding a fine powder.

The solventborne alkyd clear coating (as reference) and the alkyd-MMT composite coating with 3 wt.% MMT nanoclay were prepared and coated on panel samples of carbon steel by Arkema, France. To have an optimal film formation, varnishes based on alkyd and alkyd with nanoclay were applied on cold rolled carbon steel with a barcoater in order to get a film thickness around 10 μm. The coated panels were kept for at least two weeks at 23 ºC – 50% RH and then another week inside a desiccator under dry atmosphere at room temperature. Small samples of 2 × 2 cm in size were cut from the coated panels and used for the AFM measurements, and larger ones were used for the EIS experiments.

The microstructure of the coatings were determined by X-ray diffraction (XRD) analysis carried out at room temperature, using a Siemens D5000 diffractometer in Bragg–Brentano geometry of an X'pert PRO PANalytical system, with CuKα radiation at a wavelength λ = 1.54 Å operated at 45 mA, 45 kV. The 2 theta (2θ) scan range was from 2° to 40°, with a step size of 0.05° and 50 second per step. The thermal stability of the coatings was evaluated by

Thermo gravimetric (TGA) analysis from 25 to 700 °C at heating rate of 20°C/min, using a PerkinElmer Pyris1 TGA Thermogravimetric Analyzer, with nitrogen as purging gas.

2.2. SEM characterization of the microstructure of the coatings

In addition to usual SEM analysis of the coating surface, for the microstructure examination, the coatings were cut horizontally by means of an In-Plane microtome; and then a chrome layer of 10 nm thickness was sputtered onto the cut surface to gain surface conductivity necessary for the SEM measurement. A SEM instrument, Zeiss Supra 40VP, was used to characterize the bulk microstructure of the reference and composite coatings, from top-view and cross-section, respectively. The SEM measurements were performed in secondary electron mode with an In-Lens secondary electron detector operated at 3 keV.

2.3. In-situ AFM measurements

An Agilent 5500 AFM with a liquid cell was employed for topography imaging, using an etched silicon cantilever and operating in contact mode. The tip type was NANOSENSORS™ PPP-CONTR, with a radius of curvature < 10 nm, and Al coating on detector side of cantilever (tip height: 10-15 μm, thickness: 2.0±1 μm, resonance frequency: 6-21 kHz, spring constant: 0.02-0.77 N/m). The AFM measurements were performed in air and then repeatedly in 3 wt.% NaCl solution after different exposure times. The scan areas were ranged from a few to 80 μm in size. *In-situ* AFM measurements were performed to investigate the micro- and nano-structure and defects of the coatings in the wet condition and their influence on the corrosion protection of the coatings, by judging the detailed surface changes observed in the corrosive solution. The roughness of the coating surface was evaluated by statistical analysis of the AFM images. The AFM images are presented with relative height values, i.e., the Z-scale shows the minimum and maximum heights of the

features on the scanned area.

Average roughness (Ra) is the arithmetical mean deviation, i.e., the average deviation of all roughness profile from a mean line over the evaluation length, and it is calculated as:[23]

$$R_a = \frac{1}{N}\sum_{j=1}^{N}|r_j|$$

Root mean square roughness (Rq) is the average of the measured height deviations taken within the evaluation length and measured from the mean line, and it is calculated as:

$$R_q = \sqrt{\frac{1}{N}\sum_{j=1}^{N} r_j^2}$$

2.4. EIS measurements during exposure

A three-electrode electrochemical cell was used for the electrochemical measurements, with the coating sample as working electrode, a saturated Ag/AgCl electrode (+0.205 V vs. SHE) as reference electrode and platinum wire as counter electrode, respectively. The exposed coating area was 0.6 cm^2. The EIS measurements were performed at the OCP in 3 wt.% NaCl solution, repeatedly after different exposure periods, using a potentiostat and frequency response analyzer. The EIS was measured in the frequency range 10^5–10^{-2} Hz, using perturbation amplitude of 5 mV. The EIS data were analyzed by using the ZView software.

3. Results and discussion

3.1. XRD spectra of the coatings

Figure 1 shows the XRD spectra of the alkyd clear coating and the alkyd-MMT composite coating, respectively. In the spectrum for the alkyd coating, the broad peak in the range 2θ = 14-30° corresponds to the amorphous state of the alkyd matrix [24]. In contrast, the spectrum

for the composite coating shows characteristic diffraction peaks in the range of 2θ = 2-10°, which give structure information of the MMT layers.

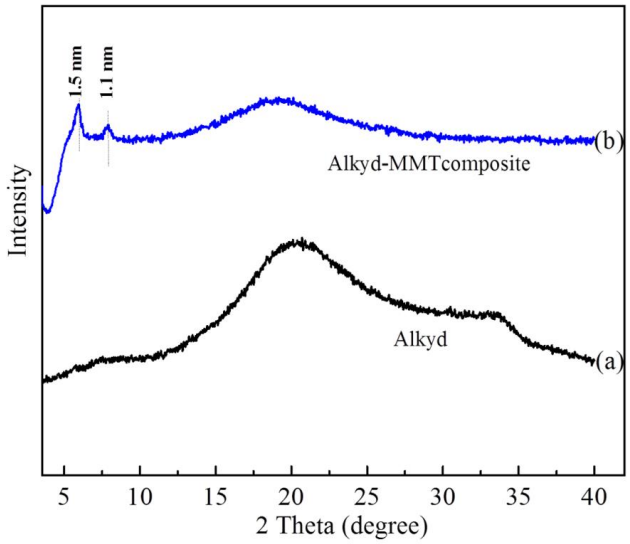

Fig. 1. XRD spectra of (a) alkyd coating and (b) alkyd-MMT composite coating.

In the XRD spectrum, the peak d_{001} corresponds to the *d*-spacing of the lamellar structure of MMT, which is calculated from Bragg's Law given in Eq. (1),

$$\lambda = 2d \sin\theta \quad (1)$$

Where λ is the wavelength of the X-ray radiation, θ the measured diffraction angle, and d the spacing between lattice planes of the MMT layers.

The two sharp peaks appearing at 2θ = 6° and 8° correspond to the d_{001} plane of the MMT platelets with a *d*-spacing of 15 Å and 11 Å, respectively. These relative large *d* space values indicate intercalated nanocomposite structure in the alkyd-MMT coating, where a single or more than one extended polymer chain is intercalated between the silicate layers, resulting in an ordered multilayer morphology [4].

These peak positions suggest that the ordered laminar MMT is present in the composite hybrids rather than exfoliated uniform nanostructure. In the other word, a part of MMT was

not homogeneously dispersed into the alkyd matrix, although the interlayer spacing was enlarged due to the intercalation of the polymer chains between the MMT layers [4][24][25].

3.2. Thermal stability of the coatings

The thermal stability of the alkyd coating and the alkyd-MMT composite coating was determined by TGA. Figure 2 shows the typical TGA curves, i.e., weight residual as a function of temperature. The onset and the end-set temperatures were established from the intersection of the two tangents, and the peak degradation temperatures were determined by the inflection points on the curves.

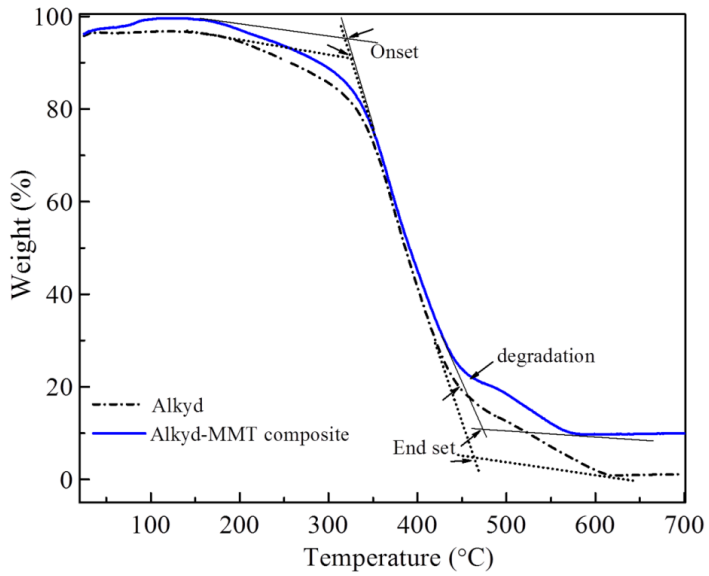

Fig. 2. TGA curves of (a) alkyd coating and (b) alkyd-MMT composite coating.

Apparently, there are two stages of weight loss for each kind of sample, starting at 164 °C and ending at 600 °C, which probably related to the degradation of some added components (e.g., surfactants) followed by the structural decomposition of the polymer matrix at the high temperature range [4][15]. Judged from the degradation step of the alkyd matrix in the TGA curves, the alkyd-MMT composite coating degrades at the temperature of 458 °C, which is

ca. 10 °C higher than the degradation of the alkyd coating. And, the end-set temperature is 462 °C for the composite coating while it is 455 °C for the alkyd coating. The increase in the onset and end-set temperatures of thermal decomposition of the alkyd-MMT composite coating indicates an improved thermal stability of the composite coating as compared to the alkyd coating. Meanwhile, this relatively small change of the composite coating suggests the intercalation structure in the composite coating instead of exfoliation, which can give a large interfacial interaction between the alkyd and nanoclay and enhance the barrier property [24][26].

The enhancement of thermal stability of the alkyd-MMT composite coating may be attributed to that, firstly, some of the active centres of the alkyd main chains become inactive for decomposition when they are in contact to the nanoclay. Secondly, the interactions between alkyd matrix and the nanoclay prevent unzipping degradation of the alkyd chains by increasing the physical and chemical crosslinking points built up between the polymer chains and nanoclay particles [4][15][24][25][27]. Since an optimal amount of nanofiller plays an important role for determining the extent of the improvement of thermal stabilization of nanocomposites [4], it is interesting to further study the influence of MMT content on the thermal stability of alkyd-MMT composite coating.

3.3. Micro- and nano-structure of the coatings

Figure 3 displays the SEM micrographs of the cross-section of the alkyd coating and the alkyd-MMT composite coating, respectively. The alkyd coating shows a continuous network-like appearance (Fig. 3(a)) caused by microtome cutting; and no particle or agglomeration could be observed even at a high magnification (Fig. 3(b)). Adding 3 wt.% MMT nanoclay into the alkyd coating caused remarkable change in the microstructure of the coating. The dispersion of MMT is not very homogeneous in the composite coating, and there are particle

agglomerates which tend to localize on the surface layer of the alkyd matrix, as shown in the top view image of Fig. 3(c). Figure 3(d) displays a typical cross section image of the alkyd-MMT composite coating, showing dense population of MMT with laminar structure of a few μm in length. Figure 3(e) shows a high magnification image of the laminar sheets, with thin edge of nm thickness. This kind of laminar structure is beneficial for the improvement of barrier and mechanical properties, especially for polymer-silicate nanocomposite coatings at low particle loading [6][28].

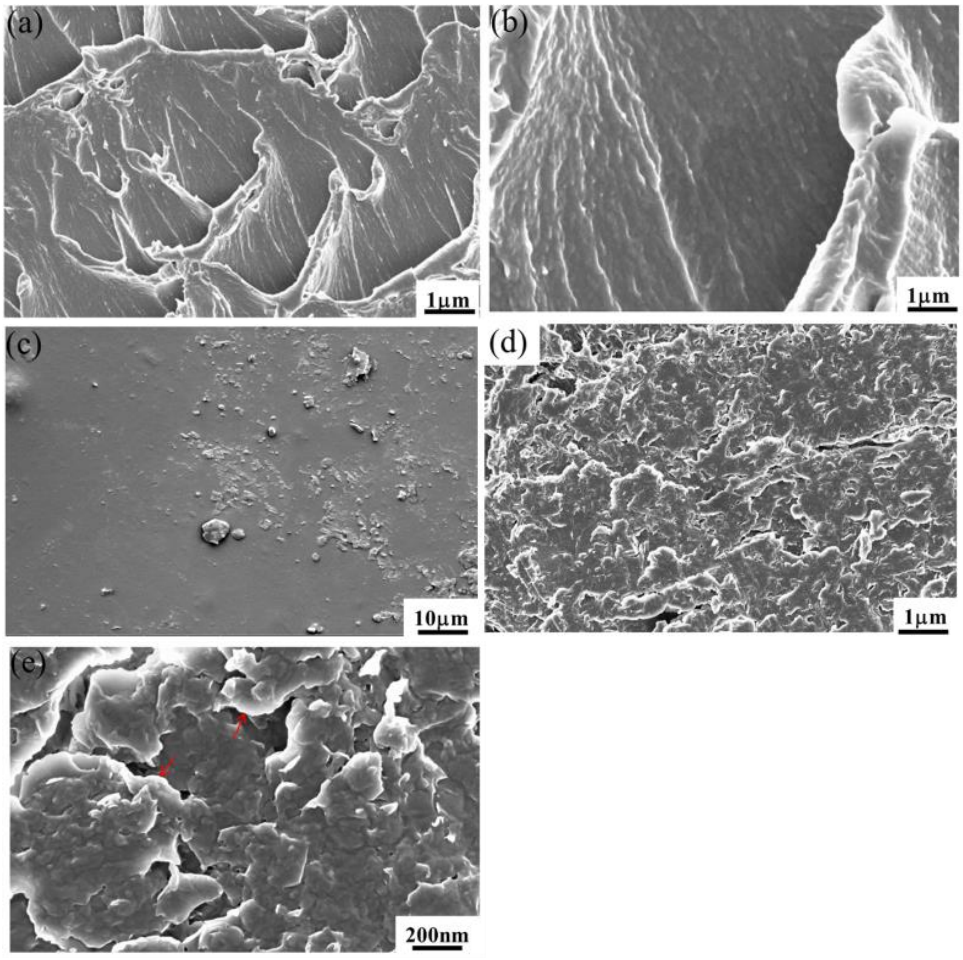

Fig. 3. SEM micrographs of the cross-section of (a, b) alkyd coating, and (c, d) the alkyd-MMT nanocomposite coating.

The addition of MMT nanoclay into the alkyd matrix may reduce the voids and improve the

performance of the coating because, firstly, the cross linking between nanoclay and alkyd could take place when the nanoclay is intercalated in the resin matrix [24], enhancing the barrier and mechanical properties; secondly, the MMT sheets can partially block the pores in the coating by arranging themselves parallel to the metal surface [29], effectively impeding the water permeation. Thus, the alkyd-MMT composite coating is expected to provide a better barrier corrosion protection than the alkyd coating. However, some nano-sized cracks may be formed in the composite coating due to pronounced agglomeration of the MMT sheets in the coating, as can be seen in Fig. 3(d-e). This may reduce the positive effect of the MMT additive in the composite coating.

3.4. Ex-situ and in-situ AFM study

Figures 4(a-e) show the AFM images for the alkyd coating in air and the sequential *in-situ* AFM images obtained in 3 wt.% NaCl solution. As shown in Fig. 4(a), in addition to hills and valleys, there are defects such as pinholes and micro-cracks in the coating (marked by dot circles), and Fig. 4(b) shows more clearly the pinholes. The pinholes and micro-cracks can become easy pathways for penetration of water and corrosive ions. The coating surface is relative smooth, with a roughness value ca. 20 nm on an area of 80 μm in size.

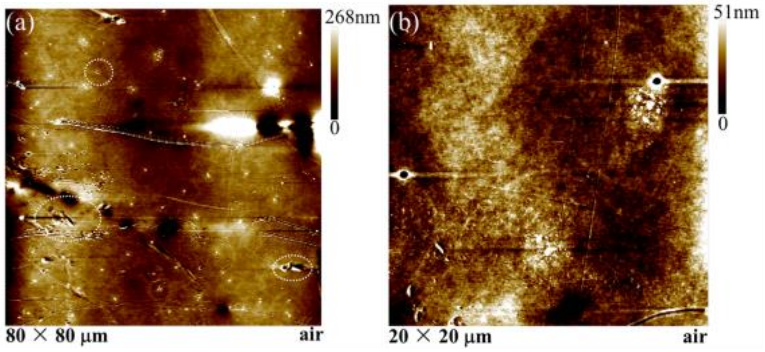

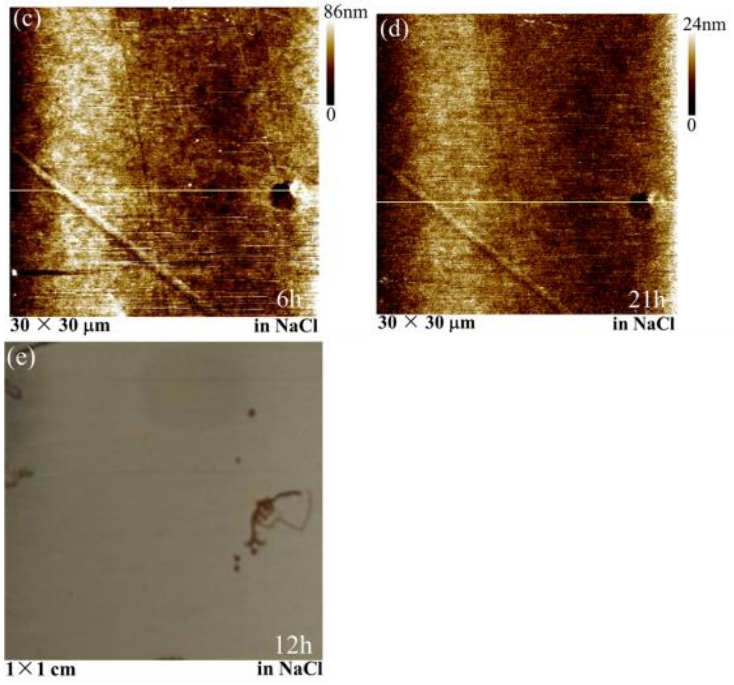

Fig. 4. *Ex-situ* and *in-situ* AFM images of the alkyd coating obtained in air (a, b) and in 3 wt.% NaCl solution (c, d), respectively. A photo (e) of the alkyd coating was taken after 12 hours exposure. The statistic roughness, pinhole diameter/depth and Z-scale values are given in Table 1.

Table 1. Statistic roughness, pinhole diameter/depth and Z-scale values of the alkyd coating.

The sequential *in-situ* AFM images in Figs. 4(c-d) show that, the coating surface changed significantly during 21 hours immersion in the NaCl solution, the diameter and depth of the shallow pinhole, the roughness and Z-scale of the coating surface decreased with the exposure time (Table 1), implying a low stability of the coating. These changes are probably caused by the water uptake occurred during this relative short immersion. For this thin alkyd coating, the electrolyte may diffuse through the coating and even reach to the interface between the coating and metal substrate within a relative short period. It has been reported that small defects generated during solvent evaporation and drying phase can constitute a preferential pathway for water and corrosive ions [20][30]. The photo of the alkyd coating

(Fig. 4(e)) taken after 12 hours exposure shows some brownish corrosion products, most likely red rust formed due to a fast transport of the electrolyte through the coating [11][31].

Figures 5(a-e) show the AFM images for the alkyd-MMT composite coating in air and the sequential *in-situ* AFM images obtained in 3 wt.% NaCl solution, respectively. The AFM images show very different morphology of the alkyd-MMT composite coating as compared to that of the alkyd coating. As can be seen in Figure 5(a), small and large MMT particles with hundreds nanometres to several micrometres in size distribute all over the coating surface, and there are also pinholes and micro-cracks, but in small population. A higher resolution image (scan size of 20 μm) in Fig. 5(b) shows dense population of MMT particles and some aggregates distributing over entire surface. The apparent size (sticking out on the surface) of the MMT particles is in the range of 200 nm to 1.5 μm. The statistic roughness and Z-scale values (Table 2) indicate that the alkyd-MMT composite coating is rougher than the alkyd coating. It was reported that the MMT nanoclay can migrate onto the steel surface through the solventborne resin before the cross-linking step [18], so a rough interface could be expected. Since the anchor effect is increased with the increase of surface roughness, which in turn strongly influences the adhesive properties [21], it can be inferred that the adhesion strength of the alkyd-MMT composite coating on the metal substrate should be higher than that of the alkyd coating.

The sequential in-situ AFM images of the composite coating, Figs. 5(c-e), show detailed morphology of the alkyd-MMT composite coating surface during the exposure in the NaCl solution. No considerable change of the coating surface was observed, the variation of the Z-scale was quite small, and the roughness of the coating surface remained to be almost the same during 33 hours exposure in the solution. Moreover, the line profiles across a large particle (or aggregate) marked in the images are shown in Fig. 5(f). Both the height and the

position of the particle (or aggregate) remained to be almost the same during the exposure, indicating a good stability of the MMT nanoclay in the alkyd matrix.

These *in-situ* AFM observations demonstrate excellent stability of the alkyd-MMT composite coating and suggest a reduced water penetration. A photo of the composite coating sample (Fig. 5 (g)), taken after 2 days exposure in the NaCl solution, shows no sign of corrosion products, in contrast to that appeared on the alkyd coating after only 12 hours. It was reported that the corrosion protection of polymer coatings can be improved by the addition of nanoclay because the intercalated nanoclay in the matrix can block the defects in the coating and fortify coating adhesion, and thus enhance the barrier properties [31]. These *in-situ* AFM results provide evidences that the intercalated MMT nanoclay in the alkyd matrix can reduce the water penetration and thus postpone the onset of corrosion reaction.

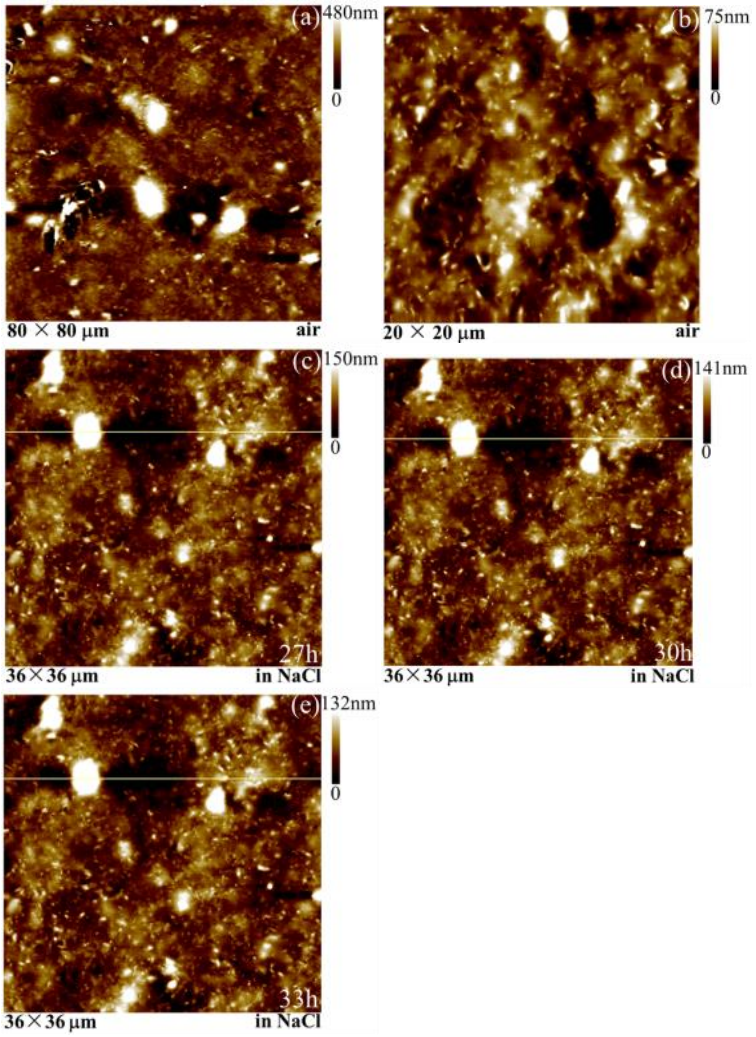

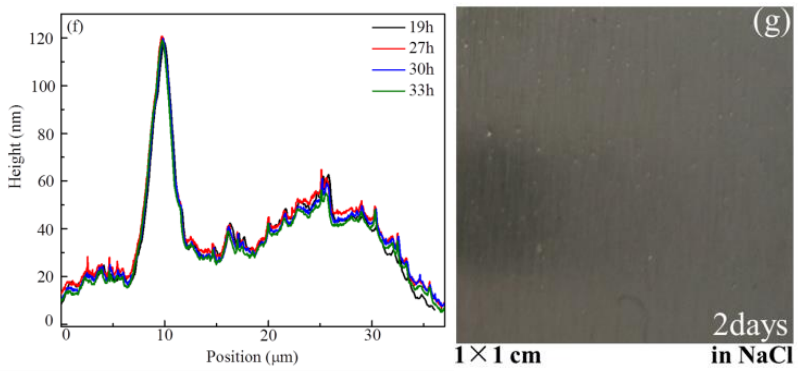

Fig. 5. *Ex-situ* and *in-situ* AFM images of the alkyd-MMT composite coating obtained in air (a, b) and in 3 wt.% NaCl solution (c, d, e), respectively. (f) Line profiles across a large particle (or aggregate) marked in the images. The statistic roughness and Z-scale values are given in Table 2. The photo was taken after 2 days exposure in 3% NaCl solution.

Table 2. Statistic roughness and Z-scale values for the alkyd-MMT composite coating.

3.5. EIS evaluation of the coatings

The Bode plots of the alkyd coating and alkyd-MMT composite coating are displayed in Figs. 6(a) and 6(b), respectively. For the alkyd coating, the impedance modulus spectrum obtained at the beginning of exposure shows a very high resistance of about 10^{10} ohm.cm^2 at low frequency range. However, it decreased rapidly with time down to the level of 10^8 ohm.cm^2 after one hour of the exposure, and a second time constant feature appeared in the low frequency range associated to the onset of corrosion process, suggesting a fast degradation of the alkyd coating due to easy water penetration in the coating [31][32].

Figure 6(b) displays the EIS spectra for the alkyd-MMT composite coating, showing only small change occurred during the exposure. The second time constant feature appeared after a longer exposure time and was not as pronounced as the alkyd coating. The EIS results indicate a beneficial effect of the intercalated MMT nanoclay on the stability of the

composite coating in the corrosive solution, in agreement with the *in-situ* AFM observations. The level of the low frequency impendence is of the order of 10^8 – 10^9 ohm.cm^2, probably the presence of micro-cracks in the composite coating (Fig. 5(a)) prevent the coating to achieve a very high impedance level. Interestingly, after initial (a few hours) slight decrease, the low frequency impendence increased with time to a value close to that measured at the very beginning of exposure. This is probably related to the formation of partially insoluble corrosion products at the metal/polymer interface which close the micro-pores [19]. For an easy comparison, the evolution of the impendence modulus at 0.015 Hz for the coatings is shown in Fig. 6(c).

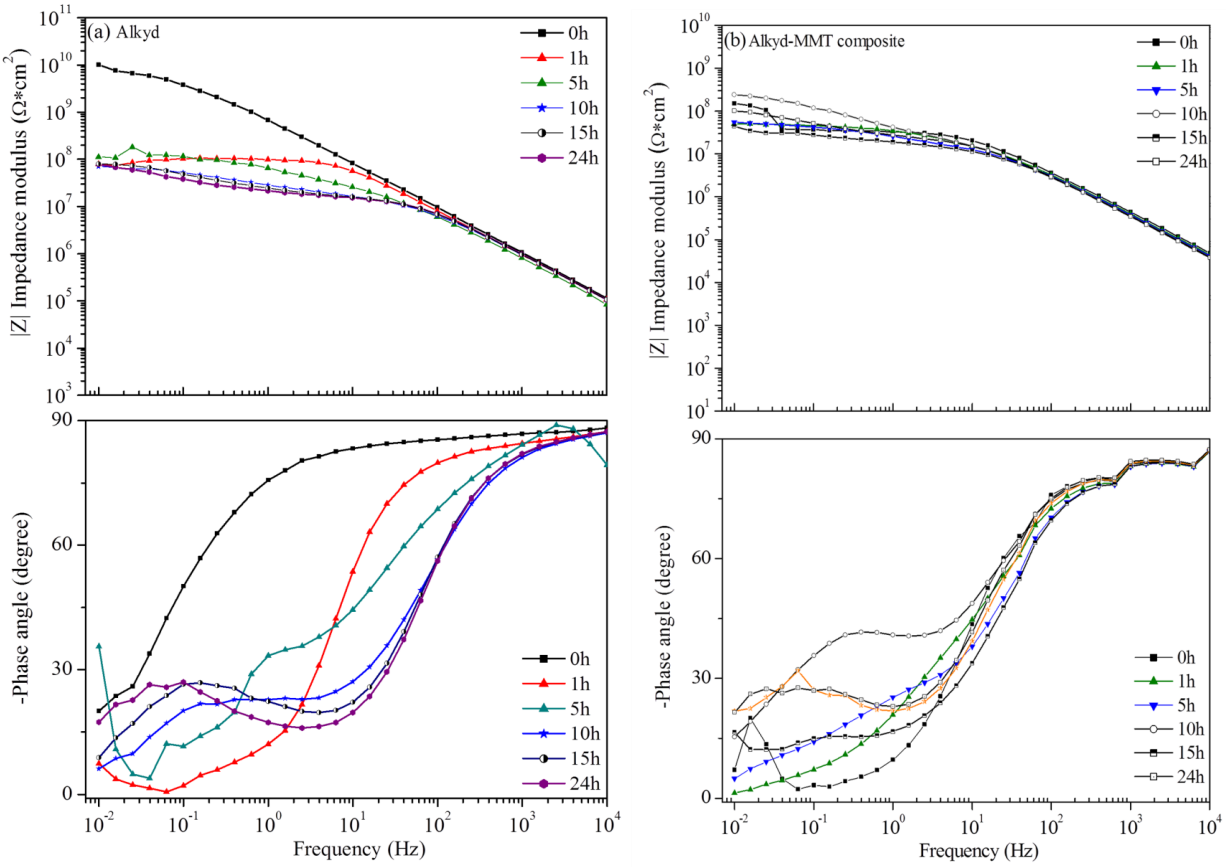

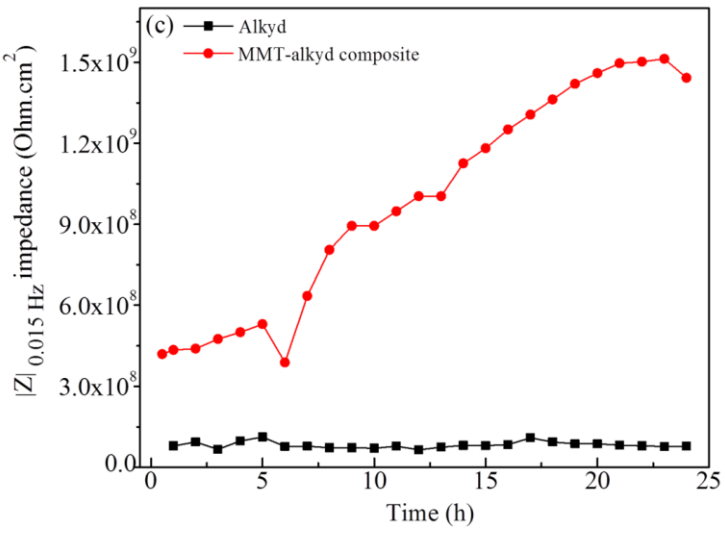

Fig. 6. Bode plots of the EIS spectra obtained for the (a) alkyd clear coating and (b) composite coating, (c) Evolution of the measured resistance at 0.015Hz for the coating samples during exposure in 3% NaCl solution.

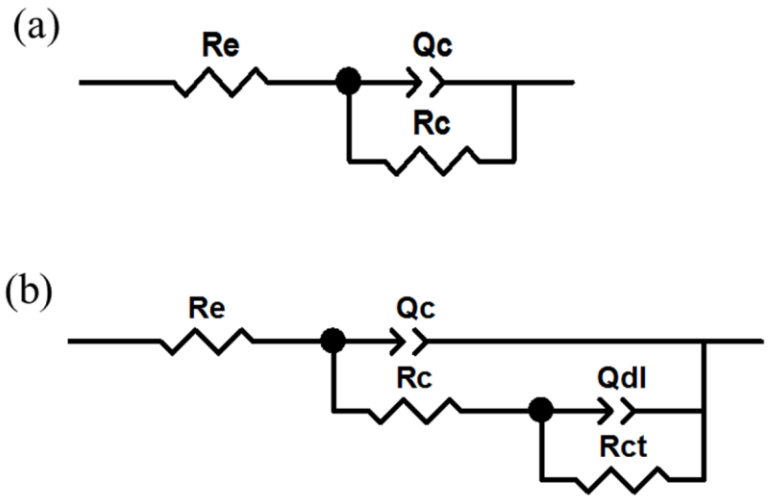

Fig. 7. Equivalent circuits for used fitting the EIS spectra.

For quantitative analysis of the spectra, two equivalent electrical circuits shown in Fig. 7 were used for spectra fitting. The circuit (a) was used for fitting of spectra exhibiting one

time constant feature and circuit (b) used for the spectra showing two time constants feature. A constant phase element (CPE) was used as a substitute of a capacitance to account for the non-ideal capacitive response from the interface. In the equivalent circuits, R_e stands for the electrolyte resistance between the reference electrode and working electrode, R_c is the coating resistance, and Q_c refers the CPE associated to the coating capacitance, R_{ct} is the charge transfer resistance and Q_{dl} is the CPE associated to the double layer capacitance.

Table 3 summarizes the fitting results, showing the evolution of Q_c and R_c for each kind of coating over the time of exposure. For the alkyd coating, during one day of exposure the R_c value decreased significantly down to the level of ca. 5×10^5 ohm.cm^2, which clearly indicates the ingress of water and ions [33]. Whereas, the R_c value of the alkyd-MMT composite coating remained to be > 10^6 Ωcm^2 during the exposure, and it increased again to the initial level after some decrease, suggesting an enhanced stability of the composite coating. It was reported that crosslinking of the matrix is increased when the silicate layers are intercalated in a polymer matrix due to the conformational effects at the clay-matrix interface [4]. The MMT nanoclay can reduce the water transport due to that the greater aspect ratio of nanoclay forces corrosive agents to travel a longer tortuous pathway before reaching the metal substrate [32]. Besides, the formation of corrosion products underneath the composite coating may partially close the micro-pores inside the coating at the metal/coating interface, which also contributes to the improved corrosion protection of the alkyd-MMT composite coating.

Table 3. Fit data for the coatings obtained from EIS spectra fitting

Based on the XRD and TGA analysis and the *ex-situ* and *in-situ* AFM observations, the enhancement of the stability and corrosion protection of the solventborne alkyd-MMT composite coating may be explained by the intercalated MMT nanoclay with lamellar

structure, which acts as nanofiller to increase the cross linking of the matrix due to the conformational effects at the clay-matrix interface, to decrease the defects and porosity of the coating by reacting with the alkyd matrix before or during the curing process, thus significantly reduce the water transport and improve the barrier property and corrosion protection of the polymer-silicate composites [4][13][29][31][34].

4. Conclusions

In this study, the effect of addition of 3 wt.% MMT nanoclay on the corrosion protection of a solventborne alkyd coating has been investigated by microstructure characterization, *in-situ* AFM observation and EIS evaluation in 3 wt. % NaCl solution.

The XRD analysis suggests a certain interaction between layered silicate and alkyd matrix, resulting in an intercalated nanostructure of the alkyd-MMT composite coating. The TGA results show a positive shift of the thermal decomposition temperature, indicating an improved thermal stability of the alkyd-MMT composite coating. The cross-sectional SEM micrographs of the composite coating reveal the distribution of the MMT layered nanoclay and also aggregates inside the coating.

The AFM images show uniform distribution of the layered MMT sheets and aggregates in the composite coating. Both the *in-situ* AFM observations and the EIS measurements in 3 wt.% NaCl solution demonstrate excellent stability of the alkyd-MMT composite coating, and suggest an improved corrosion protection of the alkyd-MMT composite coating on carbon steel as compared to the alkyd coating. The enhanced corrosion protection of the alkyd-MMT composite coating is attributed to the beneficial effects of the intercalated lamellar MMT nanoclay, improving the barrier properties of the coating by blocking the defects and decreasing the water transport in the composite coating.

Acknowledgments

Financial support from the European Union's Seventh Framework Programme for research, technological development and demonstration under grant agreement No. SteelCoat 263262 is highly acknowledged. Dr. Karin Persson and Karin Hallstensson at SP Technical Research Institute of Sweden Chemistry, Stockholm, Sweden, are acknowledged for the help with TGA analysis. Dr. Inna Soroka at Applied Physical Chemistry, KTH Royal Institute of Technology is acknowledged for the help with XRD analysis.

References

[1] E.G. Bobalek, E.R. Moore, S.S. Levy, C.C. Lee, Some implications of the gel point concept to the chemistry of alkyd resins, J. Appl. Polym. Sci. 8 (1964) 625–657. doi:10.1002/app.1964.070080207.

[2] A.M. Atta, R.A. El-Ghazawy, A.M. El-Saeed, Corrosion Protective Coating Based on Alkyd Resins Derived from Recycled Poly (ethylene terephthalate) Waste for Carbon steel, Int. J. Electrochem. Sci. 8 (2013) 5136–5152.

[3] T.J. Pinnavaia, Intercalated clay catalysts., Science. 220 (1983) 365–371. doi:10.1126/science.220.4595.365.

[4] M. Alexandre, P. Dubois, Polymer-layered silicate nanocomposites: preparation, properties and uses of a new class of materials, Mater. Sci. Eng. R Reports. 28 (2000) 1–63. doi:10.1016/S0927-796X(00)00012-7.

[5] E.P. Giannelis, R. Krishnamoorti, E. Manias, Polymer-Silicate Nanocomposites: Model Systems for Confined Polymers and Polymer Brushes, Adv. Polym. Sci. 138 (1999) 107–147. doi:10.1007/3-540-69711-X.

[6] S. Pavlidou, C.D. Papaspyrides, A review on polymer–layered silicate nanocomposites, Prog. Polym. Sci. 33 (2008) 1119–1198. doi:10.1016/j.progpolymsci.2008.07.008.

[7] J.-M. Yeh, C.-T. Yao, C.-F. Hsieh, L.-H. Lin, P.-L. Chen, J.-C. Wu, et al., Preparation, characterization and electrochemical corrosion studies on environmentally friendly waterborne polyurethane/Na+-MMT clay nanocomposite coatings, Eur. Polym. J. 44 (2008) 3046–3056. doi:10.1016/j.eurpolymj.2008.05.037.

[8] S.-A. Gârea, H. Iovu, A. Bulearca, New organophilic agents of montmorillonite used as reinforcing agent in epoxy nanocomposites, Polym. Test. 27 (2008) 100–113. doi:10.1016/j.polymertesting.2007.09.009.

[9] G. Gorrasi, M. Tortora, V. Vittoria, E. Pollet, B. Lepoittevin, M. Alexandre, et al., Vapor barrier properties of polycaprolactone montmorillonite nanocomposites: effect of clay dispersion, Polymer (Guildf). 44 (2003) 2271–2279. doi:10.1016/S0032-3861(03)00108-3.

[10] M.-G. Olivier, M. Fedel, V. Sciamanna, C. Vandermiers, C. Motte, M. Poelman, et al., Study of the effect of nanoclay incorporation on the rheological properties and corrosion protection by a silane layer, Prog. Org. Coatings. 72 (2011) 15–20. doi:10.1016/j.porgcoat.2010.11.022.

[11] M.R. Bagherzadeh, T. Mousavinejad, Preparation and investigation of anticorrosion properties of the water-based epoxy-clay nanocoating modified by Na+-MMT and Cloisite 30B, Prog. Org. Coatings. 74 (2012) 589–595. doi:10.1016/j.porgcoat.2012.02.006.

[12] F. Deflorian, S. Rossi, M. Fedel, C. Motte, Electrochemical investigation of high-performance silane sol–gel films containing clay nanoparticles, Prog. Org. Coatings. 69 (2010) 158–166. doi:10.1016/j.porgcoat.2010.04.007.

[13] J. Yeh, C. Chin, Structure and properties of poly(o-methoxyaniline)-clay nanocomposite materials, J. Appl. Polym. Sci. 88 (2003) 1072–1080. doi:10.1002/app.11829.

[14] J. Yeh, S. Liou, C. Lai, P. Wu, T.-Y. Tsai, Enhancement of Corrosion Protection Effect in Polyaniline via the Formation of Polyaniline−Clay Nanocomposite Materials, Chem. Mater. 13 (2001) 1131–1136. doi:10.1021/cm000938r.

[15] J. Yeh, S. Liou, C. Lin, C. Cheng, Y.-W. Chang, K. Lee, Anticorrosively Enhanced PMMA−Clay Nanocomposite Materials with Quaternary Alkylphosphonium Salt as an Intercalating Agent, Chem. Mater. 14 (2002) 154–161. doi:10.1021/cm010337f.

[16] J.-M. Yeh, H.-Y. Huang, C.-L. Chen, W.-F. Su, Y.-H. Yu, Siloxane-modified epoxy resin–clay nanocomposite coatings with advanced anticorrosive properties prepared by a solution dispersion approach, Surf. Coatings Technol. 200 (2006) 2753–2763. doi:10.1016/j.surfcoat.2004.11.008.

[17] J. Yeh, C.-L. Chen, Y. Chen, C. Ma, K. Lee, Y. Wei, et al., Enhancement of corrosion protection effect of poly(o-ethoxyaniline) via the formation of poly(o-ethoxyaniline)–clay nanocomposite materials, Polymer (Guildf). 43 (2002) 2729–2736. doi:10.1016/S0032-3861(02)00005-8.

[18] T. Thi Xuan Hang, T.A. Truc, T.H. Nam, V.K. Oanh, J.-B. Jorcin, N. Pébère, Corrosion protection of carbon steel by an epoxy resin containing organically modified clay, Surf. Coatings Technol. 201 (2007) 7408–7415. doi:10.1016/j.surfcoat.2007.02.009.

[19] R. Naderi, M. Fedel, F. Deflorian, M. Poelman, M. Olivier, Synergistic effect of clay nanoparticles and cerium component on the corrosion behavior of eco-friendly silane sol–gel layer applied on pure aluminum, Surf. Coatings Technol. 224 (2013) 93–100. doi:10.1016/j.surfcoat.2013.03.005.

[20] C. Motte, M. Poelman, A. Roobroeck, M. Fedel, F. Deflorian, M.-G. Olivier, Improvement of corrosion protection offered to galvanized steel by incorporation of lanthanide modified nanoclays in silane layer, Prog. Org. Coatings. 74 (2012) 326–333. doi:10.1016/j.porgcoat.2011.12.001.

[21] M. Ataeefard, S. Moradian, Surface properties of polypropylene/organoclay nanocomposites, Appl. Surf. Sci. 257 (2011) 2320–2326. doi:10.1016/j.apsusc.2010.09.096.

[22] W.R.B. and N. Hilal, Atomic Force Microscopy in Process Engineering, Elsevier, 2009. doi:10.1016/B978-1-85617-517-3.00014-6.

[23] E.S. Gadelmawla, M.M. Koura, T.M. a. Maksoud, I.M. Elewa, H.H. Soliman, Roughness parameters, J. Mater. Process. Technol. 123 (2002) 133–145. doi:10.1016/S0924-0136(02)00060-2.

[24] G. Lin, X. Zhang, Y. Li, W. Allen, I. Noda, J.E. Mark, Some Nanocomposites Based On a Glycerol-Derived Alkyd Resin and Layered Silicates, Mol. Cryst. Liq. Cryst. 483 (2008) 33–48. doi:10.1080/15421400801898066.

[25] S. Wang, C. Long, X. Wang, Q. Li, Z. Qi, Synthesis and properties of silicone rubber/organomontmorillonite hybrid nanocomposites, J. Appl. Polym. Sci. 69 (1998) 1557–1561. doi:10.1002/(SICI)1097-4628(19980822)69:8<1557::AID-APP10>3.0.CO;2-S.

[26] K. Yano, A. Usuki, A. Okada, T. Kurauchi, O. Kamigaito, Synthesis and properties of polyimide–clay hybrid, J. Polym. Sci. Part A Polym. Chem. 31 (1993) 2493–2498. doi:10.1002/pola.1993.080311009.

[27] D.C. Lee, L.W. Jang, Preparation and characterization of PMMA-clay hybrid composite by emulsion polymerization, J. Appl. Polym. Sci. 61 (1996) 1117–1122. doi:10.1002/(SICI)1097-4628(19960815)61:7<1117::AID-APP7>3.0.CO;2-P.

[28] G. Choudalakis, A.D. Gotsis, Permeability of polymer/clay nanocomposites: A review, Eur. Polym. J. 45 (2009) 967–984. doi:10.1016/j.eurpolymj.2009.01.027.

[29] P. Scarfato, L. Di Maio, M.L. Fariello, P. Russo, L. Incarnato, Preparation and evaluation of polymer/clay nanocomposite surface treatments for concrete durability enhancement, Cem. Concr. Compos. 34 (2012) 297–305. doi:10.1016/j.cemconcomp.2011.11.006.

[30] Y. Castro, A. Duran, J.J. Damborenea, A. Conde, Electrochemical behaviour of silica basic hybrid coatings deposited on stainless steel by dipping and EPD, Electrochim. Acta. 53 (2008) 6008–6017. doi:10.1016/j.electacta.2008.03.042.

[31] N. Arianpouya, M. Shishesaz, M. Arianpouya, M. Nematollahi, Evaluation of synergistic effect of nanozinc/nanoclay additives on the corrosion performance of zinc-rich polyurethane nanocomposite coatings using electrochemical properties and salt spray testing, Surf. Coatings Technol. 216 (2013) 199–206. doi:10.1016/j.surfcoat.2012.11.036.

[32] M. Nematollahi, M. Heidarian, M. Peikari, S.M. Kassiriha, N. Arianpouya, M. Esmaeilpour, Comparison between the effect of nanoglass flake and montmorillonite organoclay on corrosion performance of epoxy coating, Corros. Sci. 52 (2010) 1809–1817. doi:10.1016/j.corsci.2010.01.024.

[33] L.G. Ecco, J. Li, M. Fedel, F. Deflorian, J. Pan, EIS and in situ AFM study of barrier property and stability of waterborne and solventborne clear coats, Prog. Org. Coatings. 77 (2014) 600–608. doi:10.1016/j.porgcoat.2013.11.024.

[34] G.M. Russo, G.P. Simon, L. Incarnato, Correlation between Rheological, Mechanical, and Barrier Properties in New Copolyamide-Based Nanocomposite Films, Macromolecules. 39 (2006) 3855–3864. doi:10.1021/ma052178h.

Figure captions

Fig. 1. XRD spectra of (a) alkyd coating and (b) alkyd-MMT composite coating.

Fig. 2. TGA curves of (a) alkyd coating and (b) alkyd-MMT composite coating.

Fig. 3. SEM micrographs of the cross-section of (a, b) alkyd coating, and (c, d) the alkyd-MMT nanocomposite coating.

Fig. 4. *Ex-situ* and *in-situ* AFM images of the alkyd coating obtained in air (a, b) and in 3 wt.% NaCl solution (c, d), respectively. A photo (e) of the alkyd coating was taken after 12 hours exposure. The statistic roughness, pinhole diameter/depth and Z-scale values are given in Table 1.

Fig. 5. *Ex-situ* and *in-situ* AFM images of the alkyd-MMT composite coating obtained in air (a, b) and in 3 wt.% NaCl solution (c, d, e), respectively. (f) Line profiles across a large particle (or aggregate) marked in the images. The statistic roughness and Z-scale values are given in Table 2. The photo was taken after 2 days exposure in 3% NaCl solution.

Fig. 6. Bode plots of the EIS spectra obtained for the (a) alkyd clear coating and (b) composite coating, (c) Evolution of the measured resistance at 0.015Hz for the coating samples during exposure in 3% NaCl solution.

Fig. 7. Equivalent circuits for used fitting the EIS spectra.

Table 1. Statistic roughness, pinhole diameter/depth and Z-scale values of the alkyd coating.

Alkyd coating	**Scan size (μm)**	**Time (h)**	**Ra (nm)**	**Rq (nm)**	**Diameter (nm)/ depth of the pinhole (nm)**	**Z-scale (nm)**
In air	80×80	-	19	23	-	268
	30×30	-	3	4	-	66
	20×20		1	1	-	51
In NaCl solution	30× 30	6	5	6	1.3 / 8.5	86
	30× 30	21	3	4	1.1 / 7.8	24

Table 2. Statistic roughness and Z-scale values for the alkyd-MMT composite coating.

Alkyd-MMT composite coating	Scan size (μm)	Time (h)	Ra (nm)	Rq (nm)	Z-scale (nm)
In air	80×80	-	27	34	480
	30×30	-	7	9	165
	20×20	-	5	6	75
In NaCl solution	36×36	19	9	12	124
	36×36	27	9	12	150
	36×36	30	9	11	141
	36×36	33	9	12	132

Table 3. Fit data for the coatings obtained from EIS spectra fitting.

Time of exposure (hours)	Alkyd			Alkyd-MMT		
	Y_0 /Ω^{-1} cm^{-2} s^n	n	Rc / Ωcm^2	Y_0 / Ω^{-1} cm^{-2} s^n	n	Rc / Ωcm^2
0	(1.7±0.45)×10^{-9}	0.99	(1.5±0.34) ×10^7	(3.7±0.05)×10^{-9}	0.99	(3.5±0.11)×10^6
1	(6.0±2.20)×10^{-9}	0.97	(7.1±0.30) ×10^6	(3.9±0.55)×10^{-9}	0.99	(5.0±0.23)×10^6
5	(2.3±0.15)×10^{-9}	0.98	(1.3±0.10) ×10^6	(4.0±7.50)×10^{-9}	0.99	(2.4±0.10)×10^6
10	(2.1±0.25)×10^{-9}	0.99	(8.6±0.37) ×10^5	(4.4±0.75)×10^{-9}	0.99	(3.0±0.13)×10^6
15	(1.9±0.20)×10^{-9}	0.99	(4.9±0.51) ×10^5	(4.6±0.65)×10^{-9}	0.99	(1.4±0.05)×10^6
20	(1.5±0.05)×10^{-9}	0.97	(6.6±0.42) ×10^5	(4.4±0.80)×10^{-9}	0.99	(2.4±0.10)×10^6
24	(2.1±0.25)×10^{-9}	0.99	(7.3±0.39) ×10^5	(4.3±0.85)×10^{-9}	0.99	(3.2±0.14)×10^6

*The spectra of the coatings obtained at 0, 1 hour of exposure were fitted by the circuit (a), and the spectra acquired after one hour of exposure were fitted by circuit (b). The values are mean values based on three parallel measurements.